JACS
JOURNAL OF THE AMERICAN CHEMICAL SOCIETY

Communication

pubs.acs.org/JACS

Beyond Metal-Hydrides: Non-Transition-Metal and Metal-Free Ligand-Centered Electrocatalytic Hydrogen Evolution and Hydrogen Oxidation

Andrew Z. Haddad,[†] Brady D. Garabato,[†] Pawel M. Kozlowski,[†,‡] Robert M. Buchanan,*[,†] and Craig A. Grapperhaus*[,†]

[†]University of Louisville, Department of Chemistry, 2320 South Brook Street, Louisville, Kentucky 40292, United States

[‡]Visiting Professor, Department of Food Sciences, Medical University of Gdansk, Al. Gen. J. Hallera 107, 80-416 Gdansk, Poland

Supporting Information

ABSTRACT: A new pathway for homogeneous electrocatalytic H_2 evolution and H_2 oxidation has been developed using a redox active thiosemicarbazone and its zinc complex as seminal metal-free and transition-metal-free examples. Diacetyl-bis(*N*-4-methyl-3-thiosemicarbazone) and zinc diacetyl-bis(*N*-4-methyl-3-thiosemicarbazide) display the highest reported TOFs of any homogeneous ligand-centered H_2 evolution catalyst, 1320 and 1170 s^{-1}, respectively, while the zinc complex also displays one of the highest reported TOF values for H_2 oxidation, 72 s^{-1}, of any homogeneous catalyst. Catalysis proceeds via ligand-centered proton-transfer and electron-transfer events while avoiding traditional metal-hydride intermediates. The unique mechanism is consistent with electrochemical results and is further supported by density functional theory. The results identify a new direction for the design of electrocatalysts for H_2 evolution and H_2 oxidation that are not reliant on metal-hydride intermediates.

Hydrogen serves as a promising alternative carbon-free fuel and is an essential building block for industrial and agricultural processes. Nevertheless, 95% of industrial H_2 is produced via fossil-fuel cracking, which is environmentally unsustainable due to perpetual increases in atmospheric CO_2 levels and continual lowering of global carbon reserves.[1−3] Hydrogen evolution reactions (HERs) that proceed through the catalytic reduction of protons during the electrolysis of water provide an attractive, alternate route. Energy stored within H_2 can be recovered in fuel cells through the catalyzed oxidation of H_2 in the hydrogen oxidation reaction (HOR), which is the reverse HERs.

The utility of H_2 as an energy storage/recovery agent has been exploited since the earliest forms of life through reactivity at the transition-metal-sulfur cores of hydrogenase (H_2ase) with H_2 evolution favored in [FeFe]-H_2ase and H_2-oxidation preferential at [NiFe]-H_2ase.[4−6] In spite of the efficiency of these enzymes, their translation to industrial applications has been proven difficult, underscoring the need for artificial HER and HOR electrocatalysts. Platinum is the current "gold standard" because it operates at low overpotential with high turnover frequencies; however, its scarcity and high cost severely limit widespread use. Thus, a considerable effort has been directed toward earth-abundant, first-row transition-metal catalysts including the remarkable pendant-base bis(diamine) nickel complexes of Dubois and Bullock.[7,8] Furthermore, Eisenberg and Holland reported a series of metal-dithiolene complexes with the highest TOFs and lowest overpotentials of synthetic transition-metal-sulfur electrocatalysts under homogeneous conditions.[9−11] Each of these systems follows a metal-hydride pathway, and it is widely regarded that transition metals capable of forming metal-hydride intermediates are essential to the HER mechanism. Naturally, most HER electrocatalysts reported to date closely follow the archetypal DuBois and Bullock mechanism of ligand protonation, metal reduction, proton to hydride migration, and subsequent chemical/electrochemical steps leading to H_2 release.[7]

While the metal-hydride approach has led to significant advances, catalyst candidates that fall into this paradigm are limited to economically viable first-row transition-metals complexes capable of stabilizing hydrides. Moreover, few complexes of this type are reported to catalyze both HERs and HORs.[12] Recently, Haddad et al. reported a coordinatively saturated rhenium-thiolate complex that functions both as an HER and HOR homogeneous electrocatalyst through a potential ligand-centered process.[13] Inspired by our initial work, the compounds ZnL and H_2L were selected as potential HER and HOR catalysts based on the highly delocalized ligand framework, multiple protonation sites, ease of synthesis, good solubility, and low cost.

Herein, we report zinc diacetyl-bis(*N*-4-methyl-3-thiosemicarbazide) (ZnL)[14] as the first non-transition-metal electrocatalysts for both HER and HOR, while exhibiting the highest HER turnover frequency (TOF) of any proposed ligand-centered, homogeneous electrocatalyst and one of the highest TOF of any HOR electrocatalysts. Furthermore, we note the free ligand diacetyl-bis(*N*-4-methyl-3-thiosemicarbazone) (H_2L)[15] as the first example of a homogeneous, metal-free HER and/or HOR electrocatalyst with an HOR TOF comparable to ZnL (Figure 1).

Unlike many prior homogeneous catalysts that rely on oxidation state changes of transition metals associated with the generation of a metal-hydride intermediate, the non-transition-

Received: April 29, 2016
Published: June 21, 2016

DOI: 10.1021/jacs.6b04441
J. Am. Chem. Soc. 2016, 138, 7844−7847

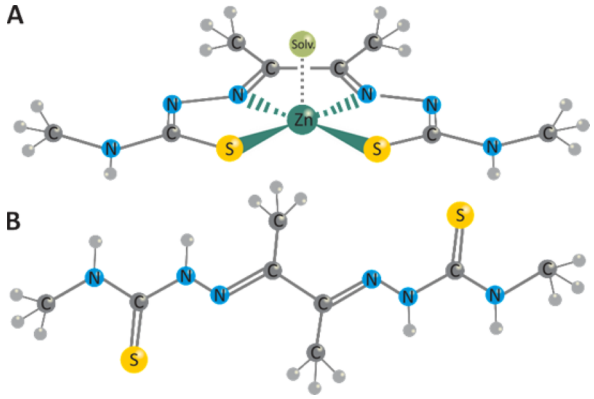

Figure 1. Ball and stick representations of electrocatalysts H_2L and ZnL. (A) Structure of ZnL with a weakly coordinating solvent molecule (yellow-green) in the axial position (Zn dark green, S yellow, N blue, C gray, H light gray). (B) Structure of H_2L (S yellow, N blue, C gray, H light gray).

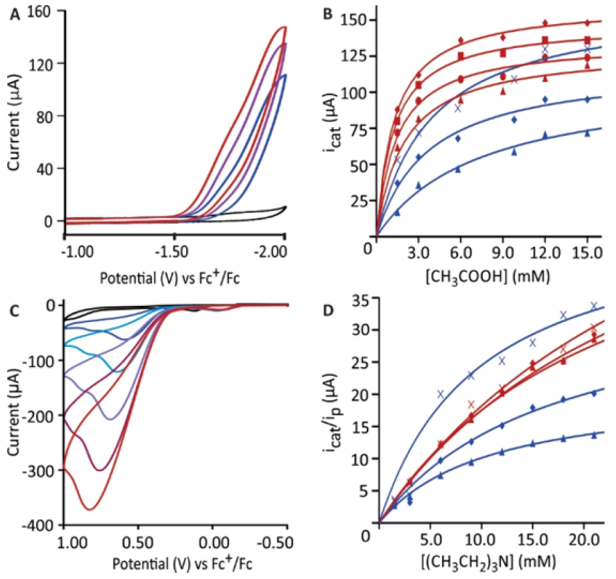

Figure 2. Electrocatalytic H_2 evolution and H_2 oxidation. (A) Cyclic voltammograms of 3 mM ZnL in methanol with no added acid (black), 6 mM CH_3COOH (blue), 9 mM CH_3COOH (purple), and 12 mM CH_3COOH (red). Data collected at a scan rate of 0.5 V/s in the presence of 0.1 M Bu_4NPF_6 as supporting electrolyte. (B) Plot of i_{cat} vs $[CH_3COOH]$ for 3 mM ZnL (red) at scan rates of 0.2 (▲), 0.3 (●), 0.4 (■), and 0.5 (◆) V/s and 3 mM H_2L (blue) at scan rates of 0.2 (▲),0.5 (◆), and 1.0 (×) V/s. (C) Cyclic voltammograms of 0.3 mM ZnL in methanol under 1 atm. H_2 with no added base (black), 3 mM $(CH_3CH_2)_3N$ (dark blue), 6 mM $(CH_3CH_2)_3N$ (light blue), 12 mM $(CH_3CH_2)_3N$ (light purple), 21 mM $(CH_3CH_2)_3N$ (dark purple), and 30 mM $(CH_3CH_2)_3N$ (red). Data collected at a scan rate of 0.5 V/s in the presence of 0.1 M Bu_4NPF_6 as supporting electrolyte. (D) Plot of i_{cat}/i_p vs $[(CH_3CH_2N)_3]$ for 0.3 mM ZnL under 1 atm. H_2 (red) and 3 mM H_2L under 1 atm. H_2 (blue) at scan rates of 0.2 (▲), 0.5 (◆), and 1.0 (×) V/s.

metal Zn(II) is redox inactive requiring redox processes to be mediated by the ligand. Recently, Thompson et al. reported an aluminum-bis(imino)pyridine complex that functions as a homogeneous HER electrocatalyst with a TOF of 3.3 h^{-1}.[16] In addition, transition-metal-free HER electrocatalysts have been reported in heterogeneous systems based on N-doped graphene (NG) with graphitic-carbon nitride ($G\text{-}C_3N_4$)[17] as well as metal-free and zinc-phthalocyanines (Zn-Pc).[18−23] Furthermore, a metal-free frustrated Lewis pair[24] HOR heterogeneous electrocatalyst has been described and is proposed to operate via a hydride intermediate, similar to Ni[12,25] and Fe[26,27] homogeneous HOR catalysts.

Solutions of ZnL in methanol or acetonitrile display catalytic hydrogen evolution upon reduction in the presence of acetic acid. In methanol, the cathodic current at −1.7 V increases with increasing acid concentration indicative of an electrocatalytic process (Figure 2A). The current plateaus at 12.0 mM acetic acid indicating acid saturation (Figure 2B) with a maximum TOF of 1170 s^{-1} at overpotential of 756 mV.[28−30] No reduction wave for ZnL is observed within the potential limits of methanol in the absence of acid, signifying that HER requires protonation prior to reduction. In acetonitrile, addition of acetic acid results in catalytic current at −2.3 V, which is near the irreversible ligand-centered reduction of H_2L in the absence of acid (Figures S1−S2) and within the range of reduction potentials previously reported for thiosemicarbizides.[31] Catalytic current is independent of acid concentration at 23 mM, yielding a higher TOF of 11700 s^{-1}, but with a larger overpotential of 1074 mV. The lower overpotential in methanol is consistent with outer-coordination sphere proton shuttling,[32] which facilitates ligand protonation prior to electrochemical reduction, as previously suggested with thiosemicarbazide complexes.[32,33] The HER TOF of ZnL is substantially higher than other proposed ligand-centered catalysts, suggesting H_2L itself may also demonstrate catalytic activity.

The metal-free H_2L ligand was subsequently evaluated as a proton reduction catalyst. H_2L displays an irreversible reduction at −2.1 V and an irreversible oxidation at +0.5 V in methanol vs Fc^+/Fc. Upon addition of acetic acid, the cathodic current at −2.1 V increases steadily (Figure S3), reaching a maximum at concentrations of 9.8 mM (Figure 2B). Under acid-saturated conditions, H_2L displays a TOF of 1320 s^{-1} with an overpotential of 1430 mV. To our knowledge, this is the only reported metal-free, homogeneous electrocatalyst for HER.

As well as electrocatalytic HER, ZnL and H_2L also catalyze HOR. Introduction of triethylamine to methanol solutions of ZnL or H_2L under 1 atm of H_2 results in an increase in anodic current near the irreversible oxidation wave of ZnL or H_2L, respectively (Figures 2C and S4). For ZnL, the catalytic current shows saturation behavior (Figure 2D) with near saturation at a base concentration of 30 mM, yielding a TOF of 72 s^{-1} with an overpotential of 315 mV. The HOR activity of H_2L ligand was similarly assessed reaching saturation at 21 mM base (Figure 2D) with a TOF of 32 s^{-1} and an overpotential of 328 mV. The HOR TOFs of ZnL and H_2L are among the highest reported of any homogeneous electrocatalyst.

The stability of ZnL as a HER electrocatalyst was further examined by controlled potential coulometry. At an applied potential of −1.7 V vs Fc^+/Fc, ZnL evolves H_2 from 12 mM acetic acid solutions in methanol with a turnover number of 37 after 2.5 h (Figure 3A) based on a total charge of 19.8 C. The identity of the gaseous product was confirmed as H_2 by gas chromatography thermal conductivity (GC-TCD). The integrated peak areas of headspace samples collected during electrolysis (Figure S5) indicate a minimum faradaic efficiency of 85%. Throughout the electrolysis, the TOF remained consistent at 15 h^{-1} with no signs of decreasing activity. Spectroelectrochemical experiments were performed on 0.1 M Bu_4NPF_6 methanol solutions of ZnL with an applied potential of

DOI: 10.1021/jacs.6b04441
J. Am. Chem. Soc. 2016, 138, 7844−7847

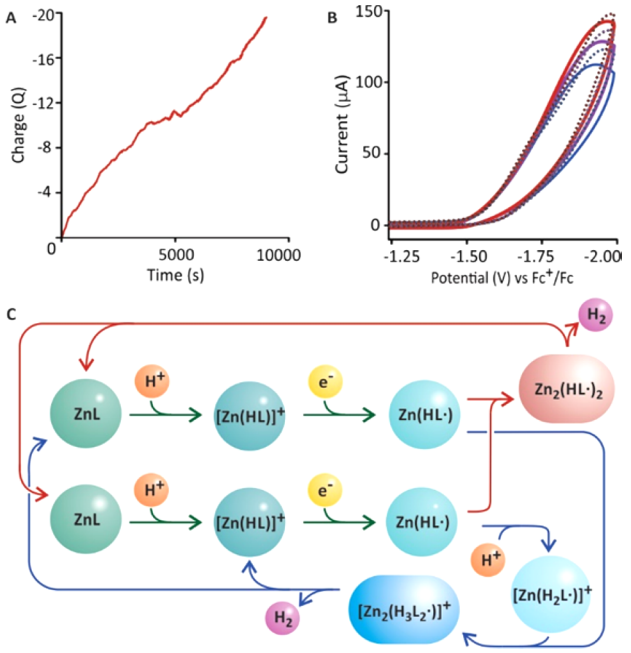

Figure 3. Mechanistic studies of H_2 evolution. (A) Plot of charge vs time recorded during bulk electrolysis of 0.1 mM ZnL and 12 mM CH_3COOH in methanol with 0.1 M Bu_4NPF_6 as supporting electrolyte. (B) Comparisons of experimental (solid) and simulated (dotted) cyclic voltammograms for 3 mM ZnL and 12 mM CH_3COOH in methanol with 0.1 M Bu_4NPF_6 as supporting electrolyte at scan rates of 0.3 (blue), 0.4 (purple), and 0.5 (red) V/s. (C) Concurrent catalytic pathways for hydrogen evolution through homocoupling of neutral Zn(HL$^\bullet$) radicals (red arrows) and heterocoupling of a neutral Zn(HL$^\bullet$) and cationic $[Zn(H_2L^\bullet)]^+$ radicals (blue arrows).

−1.7 V in order to identify the absorption characteristics of the one-electron reduced electrocatalyst, $[ZnL]^-$. UV−vis spectra were recorded before electrolysis and then measured every 15 min during electrolysis showing the growth of the absorption band near 250 nm and a decrease in the absorption band near 430 nm (Figure S18). A cyclic voltammogram was then recorded with addition of 12 mM acetic acid (Figure S19). An additional control was performed after prolonged reduction in order to rule out ligand decomposition onto electrode surface as a possible source of catalysis. After reduction, the working electrode was removed, washed with DI water, and then placed in fresh solution containing no catalyst, upon which no current was observed.

To evaluate the HER mechanism of ZnL, we first determined the rate law and measured the H/D kinetic isotope effect (KIE). Under acid-dependent conditions, the catalytic current (i_{cat}) displays a linear dependence on the square root of the scan rate indicating the current is limited by acid diffusion to the electrode surface (Figures S6−S7).[30] Further, under nonsaturating acid conditions i_{cat} is directly proportional to $[H^+]$ (Figure 2B) indicating a first-order dependence on acid concentration.[34] Varying the [ZnL] at fixed acid concentrations confirms first-order dependence at catalyst concentrations above 2 mM (Figures S8−S9). Using the deuterated acid CD_3CO_2D, the ZnL catalyst displays a small KIE of 1.2, which is distinct from the inverse KIEs reported for several metal-hydride HER catalysts and from the large KIEs associated with electrocatalysts thought to be proceeding through tunneling.[35,36]

Digital simulations of the cyclic voltammograms (Figure 3B and Table S1) reveal parallel routes to proton reduction involving homocoupling of two, neutral Zn(HL$^\bullet$) radicals and heterocoupling of a neutral Zn(HL$^\bullet$) radical with the cationic radical $[Zn(H_2L^\bullet)]^+$. The proposed mechanism (Figure 3C) begins with protonation of ZnL, $K = 2.4 \times 10^5$, followed by reduction to Zn(HL$^\bullet$), $E^\circ = -1.81$ V vs Fc^+/Fc. In the homocoupling pathway, two Zn(HL$^\bullet$) rapidly combine, $k_f = 3 \times 10^9$ M^{-1} s^{-1}, to evolve H_2 and regenerate 2 equiv of ZnL. In the alternate pathway, 1 equiv of Zn(HL$^\bullet$) is further protonated, $K = 8.8$, prior to heterocoupling. Combination of $[Zn(H_2L^\bullet)]^+$ with the second equivalent of Zn(HL$^\bullet$), $k_f = 2 \times 10^{10}$ M^{-1} s^{-1}, yields H_2 completing the catalytic cycle. The simulated kinetic and thermodynamic parameters reveal that both routes to H_2 evolution are operational across a range of experimental conditions (Figures S10−S12 and Tables S2−S3).

Density functional theory calculations using the B97-D functional and the 6-311G(d) basis set support the proposed catalytic cycle and elucidate the hydrazino nitrogen as the site of protonation. Each of the metal complexes in Figure 3C were successfully optimized (Tables S4−S6). Energies (Table S7) reveal that protonation at the hydrazino nitrogen (Figure S13) is favored by at least 13.0 kcal/mol relative to other potential basic sites within ZnL (Figures S14−S16). Evolution of H_2 through homocoupling of two Zn(HL$^\bullet$) radicals is exergonic by 42.6 kcal/mol, while the parallel pathway involving heterocoupling of Zn(HL$^\bullet$) and $[Zn(H_2L^\bullet)]^+$ releases 28.8 kcal/mol.

Analyses of the Zn(HL$^\bullet$) and $[Zn(H_2L^\bullet)]^+$ spin density profiles (Figure 4A,B) show radical character delocalized on both

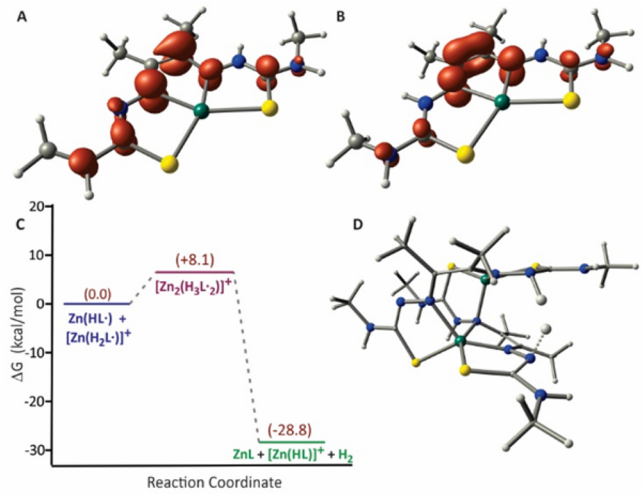

Figure 4. Energy profile along with spin densities of species involved in catalyzed H_2 evolution. Spin-density profiles for (A) Zn(HL$^\bullet$) and (B) $[Zn(H_2L^\bullet)]^+$. (C) Relative energies (ZPE corrected) for H_2 evolution through the heterocoupling of Zn(HL$^\bullet$) and $[Zn(H_2L^\bullet)]^+$ using the B97-D/6-311G(d) level of theory. (D) Structure of the singlet $[Zn_2(H_3L^\bullet{}_2)]^+$ transition state through the heterocoupling pathway. See Figure S17 for further information regarding the HER mechanism, analysis of the eigenvector associated with the imaginary frequency i1572 cm^{-1}, and the charge densities of atoms for H_2 evolution with respect to intrinsic reaction coordinate.

protonated ligand frameworks. H_2 is evolved by radical heterocoupling, overcoming an 8.1 kcal/mol barrier (Figure 4C,D). The absence of spin density on Zn for all species involved in the HER is in unequivocal support of ligand based reduction (Table S8). The transition state (TS) can be described as a dimer with H dissociations from each monomer fragment, along their respective N−H coordinates to form H_2 (Figure S17). This is consistent with N−H bond lengths in the TS of 1.25 Å for

DOI: 10.1021/jacs.6b04441
J. Am. Chem. Soc. 2016, 138, 7844−7847

$Zn(HL^{\bullet})$ and 1.36 Å for $[Zn(H_2L^{\bullet})]^+$ compared to respective equilibrium N−H distances, both of 1.02 Å. The longer N−H bond in the TS associated with $[Zn(H_2L^{\bullet})]^+$ may also be attributed to an increased charge density along the forward IRC for both N and H, compared to $Zn(HL^{\bullet})$ (Figure S17). The HER from $[Zn_2H_3L^{\bullet}{}_2]^+$ is thus interpreted as dimeric, where the now charge-reorganized $Zn(H_2L^{\bullet})$ fragment promotes early electron transfer and is coupled to proton transfer from $[Zn(HL^{\bullet})]^+$ to form H_2.

In summary, the non-transition-metal complex ZnL and the metal-free ligand H_2L represent a fundamentally new class of homogeneous HER and HOR electrocatalysts. Unlike traditional catalysts that employ a metal-hydride as the key intermediate, this new approach facilitates H_2 evolution through ligand-centered radical coupling. The combination of the redox active ligand H_2L with the non-transition-metal Zn constrains redox activity to the ligand, in contrast to transition-metal complexes where spin-coupling between the ligand radical and unpaired electrons on the metal may reduce reactivity. The confinement of radical character to the ligand is further evidenced by the catalytic activity of H_2L; albeit with higher overpotential than ZnL. The enhanced activity with Zn is attributed in part to the Lewis acidity of Zn(II), which balances the charge of the anionic ligand, promotes protonation, and lowers the reduction potential. Further, Zn(II) provides a structural framework for the N_2S_2 chelate that preorganizes the radical complexes for H_2 evolution. We can envision the strategies introduced in this study being tailored in future works to improve TOF and lower overpotential and for the development of other catalysts for small molecule activation.

■ ASSOCIATED CONTENT

Supporting Information

The Supporting Information is available free of charge on the ACS Publications website at DOI: 10.1021/jacs.6b04441.

Experimental methods and data (PDF)

■ AUTHOR INFORMATION

Corresponding Authors

*craig.grapperhaus@louisville.edu

*robert.buchanan@louisville.edu

Notes

The authors declare no competing financial interest.

■ ACKNOWLEDGMENTS

This research was supported in part by the National Science Foundation (CHE-1361728) and a grant from the Kentucky Science and Engineering Foundation as per grant agreement no. KSEF-148-502-15-350 with the Kentucky Science and Technology Corporation. The authors are thankful to Cardinal Research Cluster at the University of Louisville for providing the computational facilities. A.Z.H, R.M.B., and C.A.G. are inventors on a U.S. provisional patent application no. 62/348,420, filed by the University of Louisville Research Foundation, Inc., related to this work.

■ REFERENCES

(1) Cook, T. R.; Dogutan, D. K.; Reece, S. Y.; Surendranath, Y.; Teets, T. S.; Nocera, D. G. *Chem. Rev.* **2010**, *110*, 6474.

(2) Lewis, N. S.; Nocera, D. G. *Proc. Natl. Acad. Sci. U. S. A.* **2006**, *103*, 15729.

(3) Gray, H. B. *Nat. Chem.* **2009**, *1*, 7.

(4) Darensbourg, M. Y.; Lyon, E. J.; Zhao, X.; Georgakaki, I. P. *Proc. Natl. Acad. Sci. U. S. A.* **2003**, *100*, 3683.

(5) Fontecilla-Camps, J. C.; Volbeda, A.; Cavazza, C.; Nicolet, Y. *Chem. Rev.* **2007**, *107*, 4273.

(6) Shima, S.; Pilak, O.; Vogt, S.; Schick, M.; Stagni, M. S.; Meyer-Klaucke, W.; Warkentin, E.; Thauer, R. K.; Ermler, U. *Science* **2008**, *321*, 572.

(7) Rakowski Dubois, M.; Dubois, D. L. *Acc. Chem. Res.* **2009**, *42*, 1974.

(8) Wiese, S.; Kilgore, U. J.; DuBois, D. L.; Bullock, R. M. *ACS Catal.* **2012**, *2*, 720.

(9) McNamara, W. R.; Han, Z. J.; Yin, C. J.; Brennessel, W. W.; Holland, P. L.; Eisenberg, R. *Proc. Natl. Acad. Sci. U. S. A.* **2012**, *109*, 15594.

(10) Das, A.; Han, Z.; Brennessel, W. W.; Holland, P. L.; Eisenberg, R. *ACS Catal.* **2015**, *5*, 1397.

(11) McNamara, W. R.; Han, Z. J.; Alperin, P. J.; Brennessel, W. W.; Holland, P. L.; Eisenberg, R. *J. Am. Chem. Soc.* **2011**, *133*, 15368.

(12) Smith, S. E.; Yang, J. Y.; DuBois, D. L.; Bullock, R. M. *Angew. Chem., Int. Ed.* **2012**, *51*, 3152.

(13) Haddad, A. Z.; Kumar, D.; Ouch Sampson, K.; Matzner, A. M.; Mashuta, M. S.; Grapperhaus, C. A. *J. Am. Chem. Soc.* **2015**, *137*, 9238.

(14) Holland, J. P.; Aigbirhio, F. I.; Betts, H. M.; Bonnitcha, P. D.; Burke, P.; Christlieb, M.; Churchill, G. C.; Cowley, A. R.; Dilworth, J. R.; Donnelly, P. S.; Green, J. C.; Peach, J. M.; Vasudevan, S. R.; Warren, J. E. *Inorg. Chem.* **2007**, *46*, 465.

(15) Jones, C. J.; McCleverty, J. A. *J. Chem. Soc. A* **1970**, 2829.

(16) Thompson, E. J.; Berben, L. A. *Angew. Chem., Int. Ed.* **2015**, *54*, 11642.

(17) Zheng, Y.; Jiao, Y.; Zhu, Y.; Li, L. H.; Han, Y.; Chen, Y.; Du, A.; Jaroniec, M.; Qiao, S. Z. *Nat. Commun.* **2014**, *5*, 5.

(18) Chebotareva, N.; Nyokong, T. *Electrochim. Acta* **1997**, *42*, 3519.

(19) Koca, A. *Electrochem. Commun.* **2009**, *11*, 838.

(20) Koca, A.; Bayar, Ş.; Dinçer, H. A.; Gonca, E. *Electrochim. Acta* **2009**, *54*, 2684.

(21) Koca, A.; Kalkan, A.; Altuntaş Bayır, Z. *Electroanalysis* **2010**, *22*, 310.

(22) Koca, A.; Kalkan, A.; Bayır, Z. A. *Electrochim. Acta* **2011**, *56*, 5513.

(23) Osmanbaş, Ö. A.; Koca, A.; Kandaz, M.; Karaca, F. *Int. J. Hydrogen Energy* **2008**, *33*, 3281.

(24) Lawrence, E. J.; Blagg, R. J.; Hughes, D. L.; Ashley, A. E.; Wildgoose, G. G. *Chem. - Eur. J.* **2015**, *21*, 900.

(25) Yang, J. Y.; Chen, S.; Dougherty, W. G.; Kassel, W. S.; Bullock, R. M.; DuBois, D. L.; Raugei, S.; Rousseau, R.; Dupuis, M.; DuBois, M. R. *Chem. Commun.* **2010**, *46*, 8618.

(26) Barton, B. E.; Olsen, M. T.; Rauchfuss, T. B. *Curr. Opin. Biotechnol.* **2010**, *21*, 292.

(27) Darmon, J. M.; Raugei, S.; Liu, T.; Hulley, E. B.; Weiss, C. J.; Bullock, R. M.; Helm, M. L. *ACS Catal.* **2014**, *4*, 1246.

(28) Andrieux, C. P.; Blocman, C.; Dumasbouchiat, J. M.; Mhalla, F.; Saveant, J. M. *J. Electroanal. Chem. Interfacial Electrochem.* **1980**, *113*, 19.

(29) Fourmond, V.; Jacques, P. A.; Fontecave, M.; Artero, V. *Inorg. Chem.* **2010**, *49*, 10338.

(30) Saveant, J. M.; Su, K. B. *J. Electroanal. Chem. Interfacial Electrochem.* **1984**, *171*, 341.

(31) West, D. X.; Liberta, A. E.; Padhye, S. B.; Chikate, R. C.; Sonawane, P. B.; Kumbhar, A. S.; Yerande, R. G. *Coord. Chem. Rev.* **1993**, *123*, 49.

(32) Vuilleumier, R.; Borgis, D. *Nat. Chem.* **2012**, *4*, 432.

(33) Jing, X.; Wu, P.; Liu, X.; Yang, L.; He, C.; Duan, C. *New J. Chem.* **2015**, *39*, 1051.

(34) Hu, X. L.; Brunschwig, B. S.; Peters, J. C. *J. Am. Chem. Soc.* **2007**, *129*, 8988.

(35) Marinescu, S. C.; Winkler, J. R.; Gray, H. B. *Proc. Natl. Acad. Sci. U. S. A.* **2012**, *109*, 15127.

(36) Kotani, H.; Hanazaki, R.; Ohkubo, K.; Yamada, Y.; Fukuzumi, S. *Chem. - Eur. J.* **2011**, *17*, 2777.

DOI: 10.1021/jacs.6b04441
J. Am. Chem. Soc. 2016, 138, 7844−7847